Herrojo, Cristian; Paredes, Ferran; Mata Contreras, Francisco Javier. «Double-stub loaded microstrip line reader for very high data density microwave encoders». IEEE Transactions on microwave theory and techniques, Vol. 67 , issue 9 (Sept. 2019), p. 3527-3536. DOI 10.1109/TMTT.2019.2929128

Double-Stub Loaded Microstrip Line Reader for Very High Data Density Microwave Encoders

Cristian Herrojo, *Member IEEE*, Ferran Paredes, *Member IEEE*, and Ferran Martín, *Fellow IEEE*

***Abstract*— Compact and high-data density microwave encoders useful for motion control and near-field chipless-RFID applications are proposed in this paper. The encoders are chains of metallic strips etched on a dielectric substrate. The reader consists of a microstrip line loaded with a pair of identical open-ended folded stubs located at different positions and oriented face-to-face by their extremes. By displacing the encoder over the extremes of the stubs, inter-stub coupling arises when a strip is located on top of the stubs, thereby generating two transmission zeros (rather than one) in the frequency response of the line. Thus, the presence of a strip on top of the face-to-face stubs produces a variation in the transmission coefficient of the line, which in turn can be detected by feeding the line with a harmonic signal, conveniently tuned. Encoder motion generates an amplitude modulated (AM) signal at the output port of the line with peaks, or dips, separated a time distance dictated by the relative velocity between the reader and the encoder. Moreover, by making certain strips of the chain inoperative (e.g., by cutting them), it is possible to encode information that can be read as the absence (logic state '1') or presence (logic state '0') of peaks, or dips, at predefined positions in the output (AM) signal of the reader line. Since short strips suffice to generate inter-stub coupling, unprecedented data density per surface (DPS = 26.04 bit/cm^2) is obtained, as revealed by the implementation of 6.4 mm x 60 mm 100-bit encoders.**

***Index Terms*– Chipless-RFID, microstrip technology, microwave encoder, motion control.**

I. INTRODUCTION

MICROWAVE ENCODERS can be implemented by etching or printing metallic elements (e.g., resonators, or linear strips) at predefined positions in a dielectric substrate, typically arranged forming linear or circular chains. The working principle of such encoders is based on the detection of the presence or absence of metallic elements in the chain (revealed as peaks or dips in the output signal) when the encoder is displaced over a dedicated reader. Indeed, this working principle is similar to the one of optical encoders [1]-[3], implemented as chains of apertures in a metallic screen. However, whereas in optical encoders the presence/absence of apertures at predefined positions is detected by means of an optical beam, in microwave encoders the presence or absence of metallic elements is sensed by means of an electromagnetic signal, e.g., through near-field coupling.

Microwave encoders are of interest for motion control applications, and for the implementation of chipless radiofrequency identification (chipless-RFID) systems. In the former application, the relative velocity and displacement between the encoder and the reader is determined from the time distance between adjacent peaks, or dips, provided the chain period is known and all the metallic elements are present (and are functional) at the predefined chain positions. Both angular and linear displacement and velocity sensors based on microwave encoders (either circularly or linearly shaped) have been recently reported [4]-[8].

For identification purposes, certain metallic elements of the encoder chain are either eliminated or made inoperative. By this means, an ID code is generated, and the encoder can be used as a chipless-RFID tag, where the encoded chain replaces the application specific integrated circuit (ASIC), or chip, present in chipped-RFID tags. In these chipless-RFID systems, tags are read by proximity (through near field) by displacing them over the reader, following a time-division multiplexing scheme where the bits are read sequentially [8]-[17]. The advantage of this unconventional time-domain chipless-RFID approach is the data storage capacity, only limited by the encoder (or tag) size. Thus, chipless-RFID tags with unprecedented number of bits have been reported [8],[14],[16]. This number of bits, comparable to the one of chipped tags, is by far superior to the number of bits reported in the available literature relative to full planar chipless-RFID tags (either based on time-domain [18]-[31], frequency-domain [32]-[52], or exploiting various domains simultaneously [53]-[64]).

A figure of merit in microwave encoders for its use as linear or angular displacement and velocity sensors is the chain period, intimately related to encoder resolution. In [8],[16] microwave encoders with a period of 0.6 mm were reported. The encoder period is related to the information density per unit length (DPL), a key parameter when the encoder is used as near-field chipless-RFID tag. Note that such period corresponds to a per-unit-length data density of DPL = 16.7 bit/cm [8],[16], i.e., superior to the one achieved in [15] (DPL = 5 bit/cm), where the chain period of the encoders was 2 mm.

However, in chipless-RFID tags, the data density per surface (DPS) is also important, since it determines the area of the tag (once the number of bits is set to a certain value) and consequently tag cost. In [8], [15] and [16], the achieved data density per surface is DPS = 7.44 bit/cm^2, DPS = 1.67 bit/cm^2, and DPS = 4.9 bit/cm^2, respectively. These values are good, but the microwave encoders presented in [8],[15],[16] use metallic elements consisting of straight strips with excessive length, dictated by the

This paper is an expanded version from the IEEE Latin America Microwave Conference 2018, Arequipa, Peru, December 12-14, 2018.

This work was supported by MINECO-Spain (project TEC2016-75650-R), by *Generalitat de Catalunya* (project 2017SGR-1159), by *Institució Catalana de Recerca i Estudis Avançats* (who awarded Ferran Martín), and by FEDER funds.

C Herrojo, F. Paredes and F. Martín are with GEMMA/CIMITEC, Departament d'Enginyeria Electrònica, Universitat Autònoma de Barcelona, 08193 Bellaterra, Spain. E-mail: Ferran.Martin@uab.es.

frequency of the interrogation signal. In [15],[16], the encoder strips act as half-wavelength resonators, whereas the reader is a single stub-loaded line. In [8], the encoder strips do not behave as resonant element. However, in order to detect strip functionality (or presence/absence), the reader uses a half-wavelength resonator, and the length of the strips necessary for their detectability should be comparable to the dimensions of such reader resonator. Increasing the frequency of the interrogation signal provides a way to reduce the length of the strips, but at the expense of increasing the complexity of the reader electronics.

In this paper, we propose a new encoder-reader system, inspired by the work first presented in [15] and then optimized in [16], where the reader is a microstrip line loaded with a pair of open-ended folded stubs (oriented face-to-face by their extremes), and the encoders are chains of very short straight strips oriented orthogonally to the chain axis. The encoder strips act as narrow patch capacitors able to enhance the coupling between the stubs when such strips are located on top of the open end of the stubs. The effect is a variation in the transmission coefficient of the double stub loaded line, which is used to detect the presence/absence of functional strip in the chain (as it will be later discussed).

The working principle of the presented encoder-reader system is similar to the one reported in [8],[15],[16]. However, the encoder strips of this new system can be much shorter, provided they merely act as capacitive elements (rather than resonant elements), able to modulate inter-stub coupling. Moreover, with the proposed reader, exhibiting a frequency response with a movable pole and transmission zero (or zeros), a large excursion of the transmission coefficient at the frequency of the interrogation signal is achievable, as it will be shown. This is a fundamental aspect, with direct impact on system robustness against misalignment (between the encoder and the reader) and vibrations. Thus, the proposed system represents a significant progress as compared to previous encoder-reader systems based on encoders implemented by means of straight strips [8],[15],[16].

The work is organized as follows: the working principle of the proposed system is explained in detail in Section II, where system needs are also pointed out. Section III is devoted to analyze the proposed reader-encoder system, in order to justify the chosen reader topology, based on a double stub loaded line, in terms of encoder size, data capacity and density, and system robustness. In Section IV, the system is experimentally validated, whereas a comparison to other approaches is carried out in Section V. A tolerance analysis is carried out in Section VI. Finally, the main conclusions are highlighted in Section VII.

II. Working Principle and System Needs

The working principle of the proposed system is depicted in Fig. 1 (it is similar to the one of other near-field chiplessRFID systems [8]-[17] and displacement/velocity sensors [4]-[7], but it is reproduced here for coherence and completeness). The essential (sensitive) part of the reader is a transmission line based element sensitive to the effects of

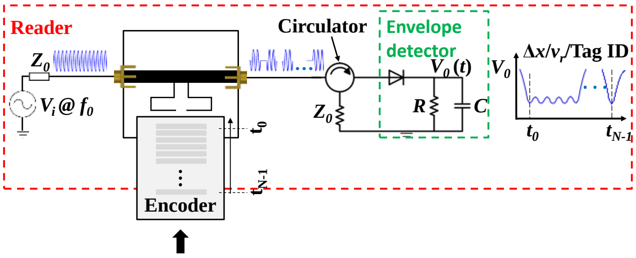

Fig. 1. Sketch of the proposed reader-encoder system.

a chain of metallic elements (the encoder) when such chain is displaced on top of the reader line at short distance. Encoder motion modulates the transmission coefficient of the line (through electromagnetic coupling), resulting in an amplitude modulated (AM) signal at the output port of the line, when it is fed by a harmonic (single tone) signal conveniently tuned. With this system, the information in regard to the relative displacement or velocity between the reader and the encoder is contained in the envelope function, with peaks, or dips, separated a time distance dictated by such velocity. For near-field chipless-RFID applications, where some elements of the encoder (i.e., those corresponding to the logic state '0') are made inoperative, the ID code is also contained in the envelope function. In this case, the relative velocity between the reader line and the encoder must be well known (for that purpose, header bits may be used). Tag reading is performed at predefined time windows, with either maxima or minima in the envelope function dictated by the presence (logic '1') or absence (logic '0') of functional metallic element on top of the reader line. To obtain the envelope function, an envelope detector is needed. The output data can be visualized in an oscilloscope [11] or, alternatively, such data can be post-processed (using a data acquisition card) [14] in order to infer either the ID code or the displacement/velocity.

In this system, encoder reading proceeds by feeding the reader line with a harmonic interrogation signal, contrary to most chipless-RFID systems, where wideband signals are typically required [18]-[64]. This aspect is important since the cost of the associated electronics of the reader can be reduced. Namely, neither narrow pulses (as needed in time-domain reflectometry based chipless-RFID systems [21],[22]), nor sweeping interrogation signals covering a wide spectral bandwidth (as used to read spectral signature barcodes [32]-[35]), are involved in the proposed system.
The frequency of the interrogation signal, f_0, must be chosen so that a large excursion of the transmission coefficient at that frequency (when the logic state switches) occurs. A significant variation of the transmission coefficient between the upper and lower value is necessary in order to obtain a high modulation index, which in turn provides system robustness against misalignments and vertical distance (air gap) variations between the reader and the encoder. However, it is also necessary that the magnitude of the upper value of the transmission coefficient is close to 0 dB, in order to guarantee a minimum (detectable) level of the envelope function. Finally, it is convenient that the transmission coefficient of the reader line exhibits as much vertical transitions as possible, with large frequency variation when the logic states switches

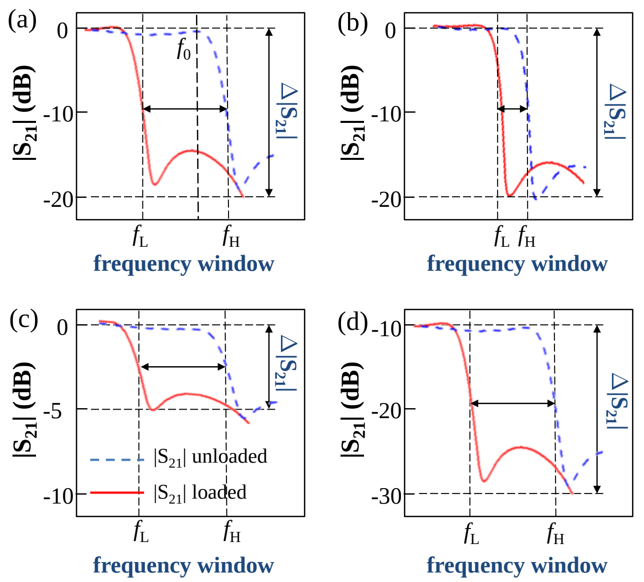

Fig. 2. Illustration of various situations of frequency responses of reader-encoder for both logic states ('0' and '1'). (a) Large transmission coefficient excursion and wide frequency window with high transmission coefficient for the upper level; (b) large transmission coefficient excursion but narrow frequency window with high transmission coefficient for the upper level; (c) small transmission coefficient excursion and wide frequency window with high transmission coefficient for the upper level; (d) large transmission coefficient excursion and wide frequency window with low transmission coefficient for the upper level.

between '0' and '1', or vice versa. This aspect results in better system robustness against fabrication related tolerances of both the line and the reader.

To further illustrate system needs, Fig. 2 schematically depicts various scenarios corresponding to different frequency responses of hypothetical readers-encoders for both logic states (i.e., with the sensitive part of the reader loaded with either functional or inoperative metallic element of the encoder). According to the previous words, the preferred case is the one of Fig. 2(a).

III. The Proposed Reader-Encoder System and Analysis

A reader-encoder structure exhibiting a frequency response of the type shown in Fig. 2(a), compatible with high data density encoders is depicted in Fig. 3. The reader, in black color, is a 50-Ω microstrip line loaded with a pair of open-ended folded stubs separated a distance l_0. The encoder, in grey color, is a chain of transversally oriented short strips etched on a dielectric substrate. When an encoder strip is located on top of the open-ended extremes of the stubs (the sensitive region), capacitive coupling between the stubs arises, resulting in a modification of the transmission coefficient useful for our purposes.

Figure 4 depicts the responses corresponding to a bare reader (i.e. without encoder strip in the sensitive region) and reader loaded with a strip. The considered substrate for the reader is the *Rogers RO4003C* with thickness h = 0.81 mm, dielectric constant ε_r = 3.55, and dissipation factor $\tan\delta$ = 0.0021. For the encoder, the considered substrate is the same as the reader but with thickness h = 0.203 mm. It can be seen that for the bare reader, the response exhibits a pole and two closed transmission zeros. By contrast, for the strip-loaded reader, further frequency splitting in the

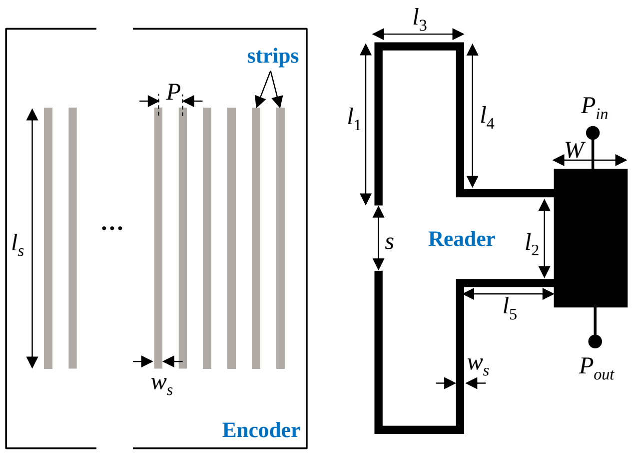

Fig. 3. Topology of the proposed reader-encoder and relevant dimensions (in mm). W = 1.81, l_0 = l_2 + w_s = 2.2, l_1 = 3.8, l_3 = 3.3, l_4 = 2.1, l_5 = 2.1, s = 1.60, P = 0.60, w_s = 0.20 and l_S = 6.4.

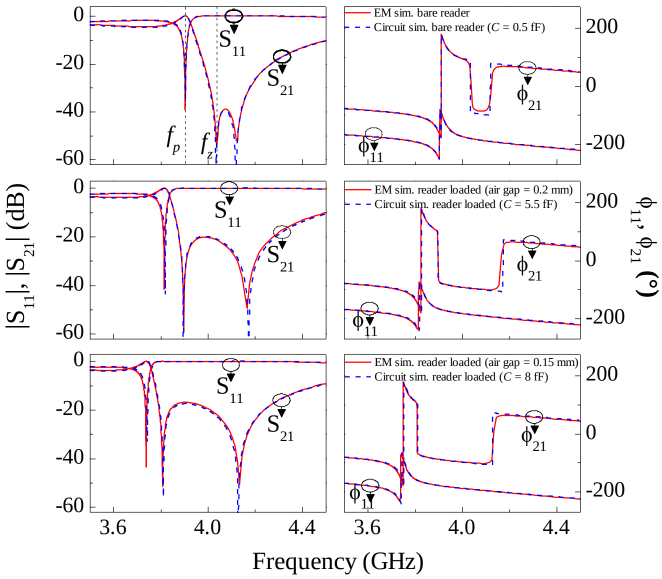

Fig. 4. Simulated frequency response (without losses) of the bare reader and reader loaded with a strip in the sensitive region. Different air gaps are considered, corresponding to different coupling capacitances (indicated). The electromagnetic simulations have been carried out with *Keysight Momentum*.

transmission zeros is visible, and the pole is displaced to lower frequencies. The splitting in the transmission zeros is indicative of certain level of coupling between the stubs, which is not totally negligible for the bare reader. Nevertheless, it is clearly manifested when a strip is located on top of the stubs, by virtue of the significant separation between the transmission zeros (note that for uncoupled stubs, the single transmission zero corresponds to the frequency where the length of the stubs is a quarter wavelength, or odd multiple).

Interestingly, the pole position in the frequency response of the bare reader roughly coincides with the first transmission zero of the response of the loaded reader (for a vertical distance between the reader and the encoder, or air gap, of 0.2 mm). By this means, a large excursion in the transmission coefficient at the pole, or transmission zero, frequency results. Thus, the frequency of the interrogation signal, f_0, must be set to a value in the vicinity of those frequencies. Obviously, the variation experienced by the transmission coefficient when a strip is located in the sensitive region of the reader depends on the air gap

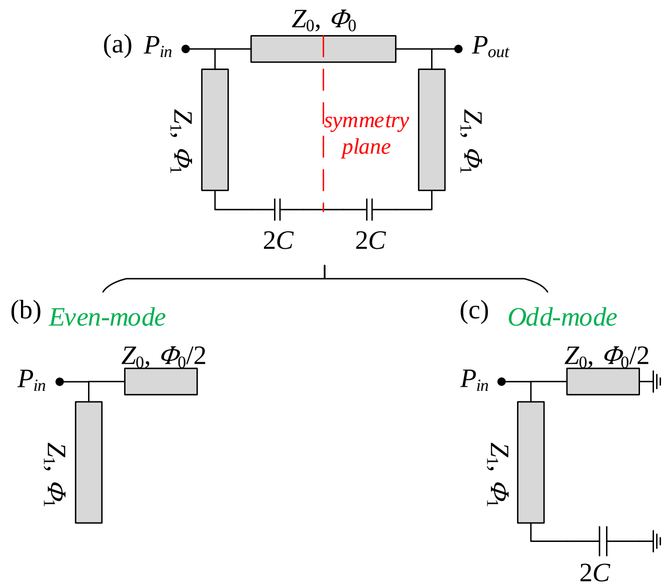

Fig. 5. Circuit schematic of the proposed reader-encoder system (a), and equivalent circuit for even-mode (b) and odd-mode (c) excitation.

separation. By further reducing such distance, inter-stub coupling increases, resulting in a progressively enhanced frequency window in the responses, as it can be seen in Fig. 4. In practice, it is difficult to accurately control the air gap separation. For that reason, it is convenient to design the reader-encoder with an appreciable frequency window for the nominal value of the air gap distance.

The positions of the pole, $\omega_p = 2\pi f_p$, and transmission zero(s), $\omega_z = 2\pi f_z$, determined by the distance between stubs, l_0, stub length, l_1, and coupling level, are important for design purposes. To gain insight on this, let us calculate the transmission and reflection coefficient of the proposed structure, modeled by the schematic depicted in Fig. 5. In that figure, C models the coupling capacitance between the stubs, ϕ_0 and ϕ_1 are the electrical length of the transmission line section (between the stub positions) and the electrical length of the stubs, respectively, and Z_0 and Z_1 are the corresponding characteristic impedances (with Z_0 = 50 Ω, as mentioned before). The model is validated by simulating the frequency response with the circuit simulator of *Keysight ADS*. The single parameter that has been adjusted in order to fit the electromagnetic simulations of Fig. 4 is the coupling capacitance. It can be seen (Fig. 4) that the agreement between the electromagnetic and circuit simulations is excellent. Thus, it is demonstrated that the effect of strips on top of the sensitive region of the reader can be modeled through capacitive coupling between the stubs.

Since the reader line is symmetric with regard to the bi-section plane between the ports, the S-parameters of the structure can be inferred from the well-known even-odd mode analysis [65]. The equivalent circuits for even- and odd-mode excitations are also depicted in Fig. 5. The reflection coefficients for the even- and odd-mode equivalent circuits are

$$\rho_e = \frac{Y_0 - Y_{in}^e}{Y_0 + Y_{in}^e} \qquad (1a)$$

$$\rho_o = \frac{Y_0 - Y_{in}^o}{Y_0 + Y_{in}^o} \qquad (1b)$$

with

$$Y_{in}^e = j\left[Y_0 \tan\frac{\phi_0}{2} + Y_1 \tan\phi_1\right] \qquad (2a)$$

$$Y_{in}^o = -j\left[Y_0 \cot\frac{\phi_0}{2} + \frac{1 + \frac{Y_1}{2\omega C}\tan\phi_1}{Z_1 \tan\phi_1 - \frac{1}{2\omega C}}\right] \qquad (2b)$$

In (1) and (2), ω is the angular frequency, $Y_0 = 1/Z_0$ and $Y_1 = 1/Z_1$ are the line admittances, and Y_{in}^e and Y_{in}^o are the admittances seen from the input ports in the even- and odd-mode circuits, respectively. The transmission and reflection coefficients of the structure of Fig. 5(a) are simply given by [65]

$$S_{21} = S_{12} = \frac{1}{2}(\rho_e - \rho_o) \qquad (3a)$$

$$S_{11} = S_{22} = \frac{1}{2}(\rho_e + \rho_o) \qquad (3b)$$

Let us now consider that C = 0 pF, corresponding to uncoupled stubs. In this case, the transmission coefficient exhibits a single transmission zero located at the frequency where $\phi_1 = \pi/2$ (and at the odd multiples). This is straightforward by inspection of the circuit model of Fig. 5(a) with C = 0 pF. Nevertheless, this conclusion is also inferred analytically, since for $\phi_1 = \pi/2$ it follows that $\rho_e = \rho_o = -1$, and consequently $S_{21} = S_{12} = 0$. As expected, the electrical length of the transmission line section between the stubs, ϕ_0, does not have any influence on the transmission zero position when C = 0 pF. However, ϕ_0 determines the location of the pole. Such pole position depends also on ϕ_1, but this parameter is dictated by the position of the transmission zero. In other words, the length of the stubs is not considered to be a design parameter, since it is fixed by the transmission zero of the bare structure, a system specification. The pole arises at that frequency satisfying $S_{11} = S_{22} = 0$, or $\rho_e + \rho_o = 0$. Since the circuits of Figs. 5(b) and (c) are purely reactive, i.e., $|\rho_e| = |\rho_o| = 1$, it follows that ρ_e and ρ_o should exhibit angles differing in π (or an odd multiple) at the frequency of the pole. According to (1) and (2), with C = 0 pF, this condition can be expressed as:

$$2\arctan\left(-\tan\frac{\phi_0}{2} - \frac{Y_1}{Y_0}\tan\phi_1\right) -$$

$$-2\arctan\left(\cot\frac{\phi_0}{2} - \frac{Y_1}{Y_0}\tan\phi_1\right) = (2n+1)\pi \qquad (4)$$

where n is an integer.

In (4), the ratio Y_1/Y_0 is not considered to be a design parameter. The reason is that $Z_0 = 1/Y_0$ = 50 Ω, as indicated before, and Y_1 is determined by the width of the stubs. Such width is set to the same value than the width of the encoder strips. By this means, inter-stub coupling caused by multiple strips simultaneously is reduced. On the other hand, the electrical length of the stubs can be expressed as

$$\phi_1 = \frac{l_1}{l_0}\phi_0 \qquad (5)$$

where it has been considered that the phase velocities (or the phase constants) of the line and stubs are identical (a reasonable approximation). Thus, expression (4) depends on a single variable, ϕ_0, provided the ratio l_1/l_0 is set to a certain value. In other words, ϕ_0 (and consequently the frequency of the pole) is dictated by the ratio l_1/l_0. However, it is not possible to isolate ϕ_0 from (4). Thus, we have obtained numerically ϕ_0 as a function of l_1/l_0 (see Fig. 6). From the value of ϕ_0, the ratio between the pole and transmission zero frequencies is given by

$$\frac{\omega_p}{\omega_z} = \frac{2\phi_0}{\pi}\frac{l_1}{l_0} \tag{6}$$

and this ratio is also depicted in Fig. 6. Thus, the relative position between the pole and the zero for the case of uncoupled stubs (C = 0 pF), is determined by the ratio between the stub length and transmission line section length.

With the pole for the bare reader (C = 0 pF) set to a certain value, ω_p, it is convenient to locate the first transmission zero frequency, ω_z', for the strip-loaded reader ($C \neq 0$ pF) at ω_p (in order to obtain a significant excursion in the transmission coefficient, as discussed before). According to (1) and (2), the condition for the transmission zero frequency with $C \neq 0$ pF is

$$2\arctan\left(-\tan\frac{\phi_0}{2} - \frac{Y_1}{Y_0}\tan\phi_1\right) - 2\arctan\left(\cot\frac{\phi_0}{2} + \frac{1}{Y_0}\frac{1+\frac{Y_1}{2\omega C}\tan\phi_1}{Z_1\tan\phi_1 - \frac{1}{2\omega C}}\right) = 0 \tag{7}$$

and it depends on C. Thus, C must be set to the value providing ω_z' = ω_p. Since at this frequency (ω_z' or ω_p), ϕ_0 and ϕ_1 are known, the single unknown in expression (7) is C, and this parameter can be obtained numerically.

The design of the reader-encoder depicted in Fig. 3 has been aided with the previous procedure. First, the transmission zero frequency of the bare structure and by considering completely uncoupled stubs (C = 0 pF) has been set to $f_z = \omega_z/2\pi$ = 4.03 GHz. This has provided the length of the stubs (l_1 = 11.3 mm in the considered substrate). The stub width has been set to w_s = 0.2 mm, identical to the width of the strips, for the reasons mentioned before. With the considered reader substrate, the characteristic impedance of the stub lines has been found to be Z_1 = 133 Ω. Then, the position of the pole for the bare reader has been set to $f_p = \omega_p/2\pi$ = 3.88 GHz, resulting in ω_p/ω_z = 0.962. With this ratio, the inter-stub distance, l_0, has been inferred from the results depicted in Fig. 6, providing l_0 = 2.33 mm (and hence l_1/l_0 = 4.85). Finally, using (7), the capacitance C has been calculated in order to obtain ω_z' = ω_p. The resulting value, C = 4.5 fF, coincides to a good approximation with the value of C given in Fig. 4, corresponding to the air gap case providing ω_z' = ω_p.

It is important to highlight that with the nominal air gap value, the encoder strip length necessary to achieve the required capacitance C is as small as 0.2 mm. Taking into account that the strip width and inter strip distance is 0.2 mm and 0.4 mm, respectively, the chain period is 0.6 mm. With these geometrical variables of the encoder, the information density per unit length is DPL = 16.7 bit/cm, identical to the one reported in [8],[16], and much better than the one reported in [15] (with DPL = 5 bit/cm). However, due to the substantially reduced length of the

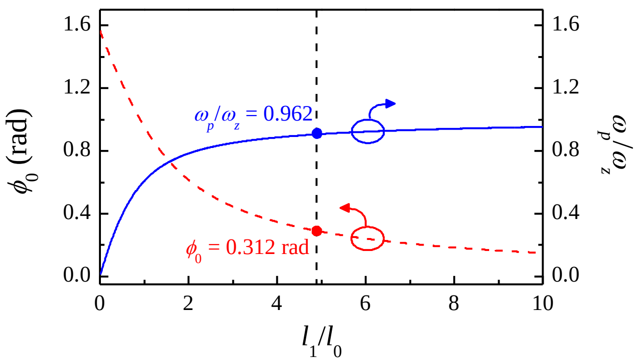

Fig. 6. Dependence of ϕ_0 and ω_p/ω_z on l_1/l_0.

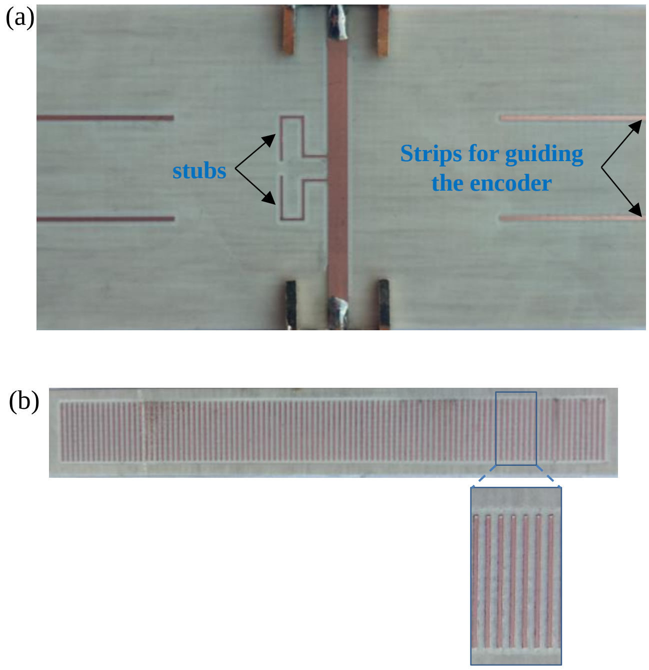

Fig. 7. Photograph of the fabricated reader (a) and 100-bit encoder with all bits set to '1' logic state (b).

strips, the data capacity per surface area achieved in this work is DPS = 26.04 bit/cm^2, i.e., 3.50, 15.6 and 5.31 times larger than those reported in [8], [15] and [16], respectively.

IV. Experimental Validation

The photograph of the designed and fabricated reader and the one of a 100-bit encoder with all the strips present, and functional, at the predefined positions are shown in Fig. 7. The reader and the tags have been fabricated by means of the milling machine *LPKF H100*. The measured response of the bare reader, inferred with the *Agilent N5221A* vector network analyzer, is depicted in Fig. 8, where it is compared with the electromagnetic simulation including losses. Such figure also includes the response of the reader with a strip on top of it. The agreement between the lossy electromagnetic simulation and the measured responses is very reasonable, taking into account the difficulty in controlling the air gap distance (nominally set to 0.2 mm) with our experimental set up.

The photograph of the experimental setup used to obtain the envelope function of the different considered encoders in response to the interrogation signal is depicted in Fig. 9.

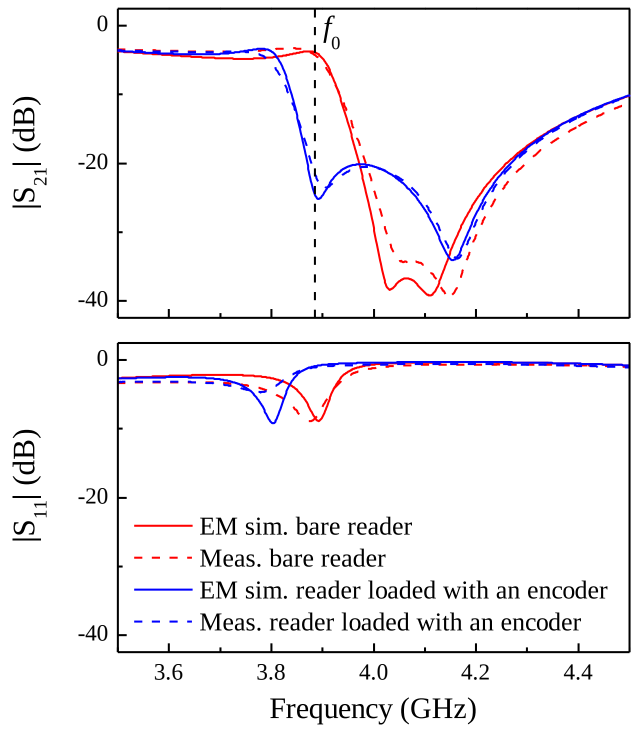

Fig. 8. Measured and simulated responses of the bare reader and reader loaded with an encoder strip on top of it.

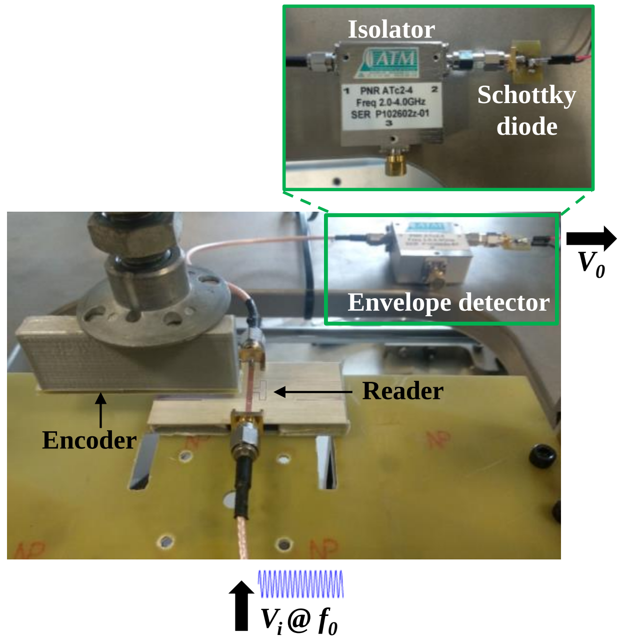

Fig. 9. Photograph of the experimental setup.

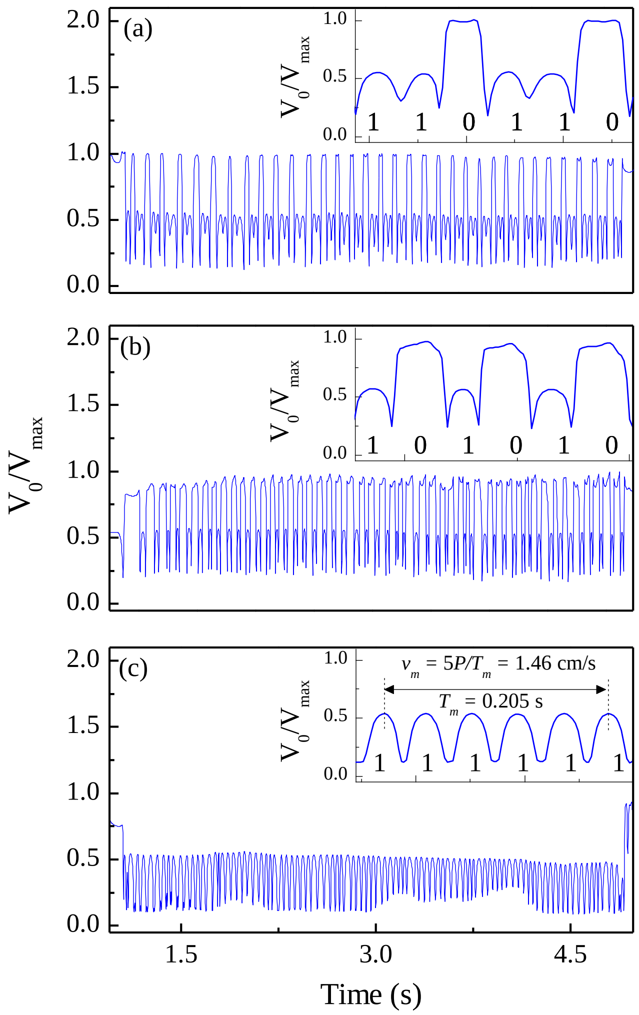

Fig. 10. Measured normalized envelope function corresponding to the indicated codes.

Such setup includes a function generator (providing the interrogation signal), an envelope detector preceded by an isolator (to avoid mismatching reflections from the diode), and an oscilloscope, where the envelope functions of the different tags are visualized. Such setup is identical to the one described in [11], where details of the specific equipment and electronic components are provided. The single difference concerns the sensitive part of the reader, a double-stub loaded line (see Fig. 7) connected between the output port of the function generator and the input port of the detector. A guiding system is used to displace at controllable distance the encoders over the sensitive part of the reader. The accuracy and robustness of such guiding system against air gap variation is limited. Nevertheless, the different encoders can be correctly read, as it will be shown next.

Three different 100-bit encoders have been used to validate the proposed approach. In all the cases, a periodic ID code has been considered, particularly, one with all bits set to '1' logic state, i.e., '11111…', one with the sequence '101010…', and one with the sequence '110110110…'. Rather than fabricating three different encoders, we have opted to program two of them after being fabricated with all bits set to '1' logic state. Namely, we have cut those strips corresponding to the logic state '0'. By this means, these strips are made inoperative, and roughly the same effect as the absence of strip on top of the sensitive part of the reader is achieved.

The envelope functions of these encoders are depicted in Fig. 10, where it can be appreciated that the different ID codes are correctly read. The interrogation signal frequency has been set to f_0 = 3.88 GHz, the frequency of the pole for the bare reader. The dynamic margin, or separation between the voltage levels corresponding to the two states, is high. However, it can be appreciated that the minimum of the envelope function does not appear exactly at the time when perfect overlapping between the encoder strip and the reader occurs. This is explained by an under air gap distance. According to Fig. 4, if the gap is below the nominal value, the coupling capacitance increases, and the response is over-shifted to lower frequencies. The result is that the first transmission zero of the strip-loaded reader no longer coincides with the pole of the bare reader (where the interrogation signal is tuned). This reduces the dynamic margin, but there is a relative position between the reader and strip where the first transmission zero coincides with the pole of the bare reader (or interrogation signal frequency). At this position, the envelope function reaches its minimum value. In view of Fig. 10 (where clearly separated voltage levels between the binary states can be appreciated), the functionality of the proposed approach for the implementation of near-field chipless-RFID systems is validated.

The functionality of the system for the measurement of linear velocities and displacements is apparent in view of Fig. 10(c). The time period of the envelope function for the '11111…' code (easily detectable, e.g., by means of a post-processing system, out of the scope of this paper) is given by the time lapse between two crosses of adjacent strips above the sensitive part of the reader. Since the spatial period is well known (0.6 mm in our case), the relative instantaneous velocity between the encoder and the reader can be easily inferred. For the envelope function of Fig. 10(a), the velocity is found to be 1.46 cm/s (actually, the instantaneous velocity slightly varies, so that such speed value has been obtained by averaging over 5 periods). The relative displacement between the reader and the encoder from a reference position is simply given by the cumulative number of peaks, or dips, in the envelope function from that position.

V. COMPARISON TO OTHER APPROACHES

The proposed system features a space resolution, which is dictated by the encoder period, i.e., 0.6 mm. The space resolution in the system reported in [8] (based on strip chain encoders, as well) was also 0.6 mm (the chain period), but the envelope function for the sequence '1111…' reported in that work does not provide significant dips/peaks. Therefore, the automatic detection of the time period (and hence the instantaneous velocity) by means of a (potential) post processing system is envisaged to be more complex. Other similar encoders, based on chains of resonant elements and used as displacement/velocity sensors have been reported [5],[7] but the achieved space resolution (2.2 mm) is not comparable to the one reported in this work.

Due to the small period achieved in the proposed encoders, the density of information per unit length is very high, particularly DPL = 16.7 bit /cm. This value is identical to the one reported in [8],[16], and much better than the one reported in [15], where DPL = 5 bit/cm. However, the most relevant aspect of these encoders is the short length of the strips. Such short length has been obtained thanks to the new designed reader, able to detect the presence or absence of functional strips of such short length on top of it. The design of such reader has represented a significant effort and constitutes the main novel aspect of this paper, as compared to previous similar works (mainly [8],[15],[16]). The information density per area unit is as high as DPS = 26.04 bit/cm^2, as it is inferred from the fact that the designed and fabricated 100-bit encoders occupy an area as small as 0.64 cm × 6 cm. This surface density, a figure of merit in chipless-RFID tags, is 3.50, 15.6 and 5.31 times larger than those reported in [8], [15] and [16], respectively, where encoders based on strip chains are also considered. As compared to other encoders based on chains of resonant elements [4]-[7],[9]-[14], the surface density obtained in the present work is significantly superior (e.g., the best DPS achieved in resonator-based encoder is the one reported in [11], with a value of DPS = 8.4 bit/cm^2).

If the comparison is extended to other chipless-RFID systems based on full planar encoders readable in time or frequency domain [18]-[64], to the best of our knowledge, the reported DPS and data capacity (number of bits) in those works are far from the values achieved in this work (as an example, a tag with DPS = 5.88 bit/cm^2 and data capacity of 64 bits is reported in [55]). Note that the number of bits (100 in the fabricated encoders) is only limited by tag size, as far as tag reading proceeds by time-division multiplexing using a harmonic interrogation signal. Further increasing the number of bits is compatible with acceptable tag dimensions and does not represent an additional complexity in the reader. In summary, an unprecedented combination of number of bits and data density has been achieved with the proposed system.

It is also remarkable the fact that the interrogation signal in the proposed system is a harmonic (single-tone) signal, rather than a wideband pulsed signal, or a sweeping frequency signal, as required in most time domain and frequency-domain, respectively, chipless-RFID systems [18]-[64]. This has direct impact in the cost associated to the reader electronics, which is reduced if wideband signals are not involved. However, the reported system requires encoder reading by proximity and proper alignment with the reader. Whereas in motion control applications this cannot be considered a limitative aspect, in certain scenarios relative to item identification, tag reading at certain distance may be necessary. In those cases, frequency-domain or traditional time-domain chipless-RFID systems may be more convenient, provided the required number of bits of the tags is not very high. However, there are applications where confidence against spying or eavesdropping is necessary, e.g., product authentication and secure paper applications. The proposed system which requires tag reading by proximity, it is inherently robust against these (potentially) malicious scenarios. Thus, as in chipless-RFID system, the proposed approach is of interest in such authentication applications, in order to avoid fraud or plagiarism in documents, high cost item products, etc.

VI. TOLERANCE ANALYSIS

In order to study the robustness of the system against air gap variations, and lateral or angular misalignment of the encoder, a tolerance analysis is needed. However, due to the difficulty to accurately control the involved geometrical parameters (namely, air gap separation and lateral or angular displacement of the encoder), such analysis is carried out at simulation level. For that purpose, a 5-bit sequence with alternating binary states is considered.

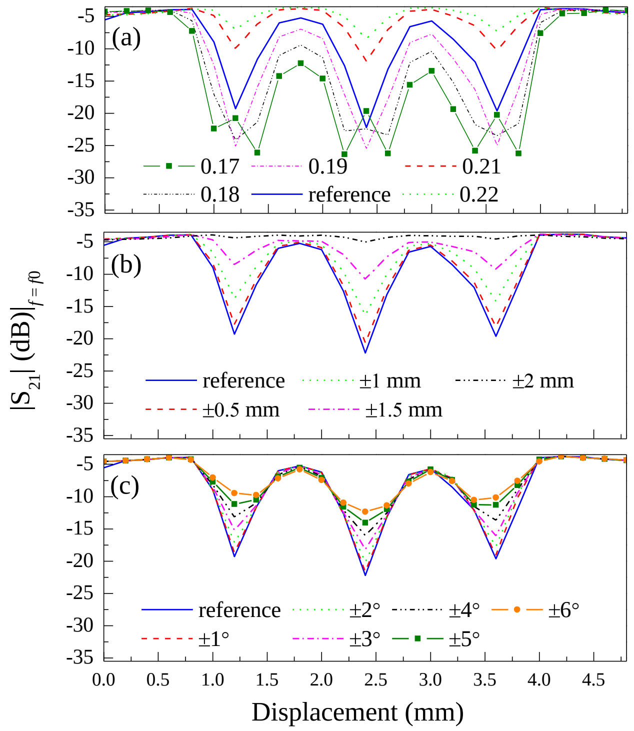

Fig. 11. Tolerance analysis. (a) Effects of the air gap variation; (b) effects of lateral misalignment; (c) effects of misalignment by encoder rotation. The curves correspond to the transmission coefficient at the frequency of the interrogation signal, as the 5-bit encoder with ID code '10101' is displaced over the reader.

The effects of the air gap variation are depicted in Fig. 11(a). It can be appreciated that the system has been optimized to operate with an air gap corresponding to the nominal value, where the excursion experienced by the transmission coefficient between the two binary states is maximum. Slightly increasing or decreasing the air gap distance reduces such excursion. According to the sensitivity of the transmission coefficient with the air gap (similar to the one reported in [8]), the mechanical guiding system for encoder motion should guarantee small variations in the air gap separation. Further robustness against the effects of the air gap can be achieved, but at the expense of larger encoder dimensions.

The effects of lateral misalignment of the encoder are shown in Fig. 11(b). According to these results, lateral displacements up to ±1 mm provide excursions in the transmission coefficient better than 8 dB. With this variation, encoder reading from the AM signal generated at the output port of the reader in response to the interrogation signal seems feasible.

Finally, Fig. 11(c) shows the effects of lack of alignment by encoder rotation, where the responses up to an angle of ±6°, with step increments of ±1°, are depicted. According to the resulting transmission coefficient variations between the two binary states, the system is tolerant up to an angle of at least ±3° (providing an excursion of the transmission coefficient of roughly 9 dB or better).

To summarize this section, the tolerances of the proposed reader-encoder system against lateral and angular misalignments are reasonable from a practical viewpoint. That is, the angular and position accuracies of the encoder guiding system in the plane of the encoder do not need to be extremely good, according to the reported tolerances. Concerning the accuracy in the orthogonal direction to the encoder and reader planes (air gap separation), the requirements are more stringent. According to the reported data [Fig. 11(a)], during encoder motion, the guiding system must guarantee an air gap separation comprised between roughly 0.17 mm and 0.22 mm. Increasing the tolerance relative to the air gap separation is possible at the expense of larger encoder sizes. Nevertheless, the fabricated encoders have been correctly read with our in-house experimental setup. Consequently, the reported air gap tolerances seem to be reasonable for an eventual reader, based on a sufficiently robust mechanical guiding system, to be used for encoder reading in a real scenario.

VII. Conclusions

In conclusion, high data density microwave encoders based on chains of transversely oriented linear strips have been proposed in this paper. The length of the strips, a critical parameter determining the data density per surface of the encoders, has been substantially reduced, as compared to previous implementations. For that purpose, a dedicated reader based on a double stub loaded microstrip line has been designed and fabricated. Such reader is able to detect the presence and functionality of the encoder strips through near-field (capacitive) coupling, when the encoder is displaced over the sensitive part of the reader (the extremes of the stubs), as needed in a reader operation. An analysis of the reader-encoder system based on the circuit schematic, where the encoder strips are modeled by means of an inter-stub coupling capacitance, has been carried out, and the model has been validated by comparison with electromagnetic simulations. Such analysis has been demonstrated to provide useful hints for design purposes. System validation has been carried out by reading several fabricated encoders with different bit combinations, where the different ID codes have been achieved by cutting certain strips of the encoder (tag programming). The functionality of the system for near-field chipless-RFID applications and for motion control (i.e., as displacement and velocity sensors) has been demonstrated. Also, a tolerance analysis, including the effects of encoder misalignment caused by lateral displacement and rotation, as well as the effects of air gap variation, has been performed through electromagnetic simulation. The obtained tolerances are reasonable in order to consider the system potentially useful for application in a real scenario. The most relevant achieved result is the information density per surface, as high as DPS = 26.04 bit/cm^2. This value, much higher than the data density obtained in other chipless-RFID systems (including near-field, time domain, frequency domain and hybrid systems), has been achieved thanks to the designed and fabricated reader, able to detect very small metallic elements (strips) in the encoder chain. To the best of our knowledge, the combination of number of bits (100 in this work) and data density per surface has never been achieved so far in microwave encoders.

References

[1] E. Eitel, "Basics of rotary encoders: overview and new technologies", *Machine Design Magazine*, 7 May 2014.

[2] G. K. McMillan, D.M. Considine, Eds., *Process Instruments and Controls Handbook*, Fifth Edition, McGraw Hill 1999, ISBN 978-0-07-012582-7, page 5.26.

[3] X. Li, J. Qi, Q. Zhang, and Y. Zhang, “Bias-tunable dual-mode ultraviolet photodetectors for photoelectric tachometer,” *Appl. Phys. Lett*., vol. 104, no. 4, pp. 041108-1–041108-4, Jan. 2014.
[4] J. Naqui, F. Martín, “Application of broadside-coupled split ring resonator (BC-SRR) loaded transmission lines to the design of rotary encoders for space applications“, *IEEE MTT-S Int. Microw. Symp.* (IMS’16), San Francisco, May 2016.
[5] J. Mata-Contreras, C. Herrojo, and F. Martín, “Application of split ring resonator (SRR) loaded transmission lines to the design of angular displacement and velocity sensors for space applications”, *IEEE Trans. Microw. Theory Techn*., vol. 65, no. 11, pp. 4450-4460, Nov. 2017.
[6] C. Herrojo, J. Mata-Contreras, F. Paredes, F. Martín, “Microwave encoders for chipless RFID and angular velocity sensors based on S-shaped split ring resonators (S-SRRs)”, *IEEE Sensors J*., vol. 17, pp. 4805-4813, Aug. 2017.
[7] J. Mata-Contreras, C. Herrojo, and F. Martín, “Detecting the rotation direction in contactless angular velocity sensors implemented with rotors loaded with multiple chains of split ring resonators (SRRs)”, *IEEE Sensors J*., vol.18, no. 17, pp. 7055-7065, Sep. 2018.
[8] C. Herrojo, F. Muela, J. Mata-Contreras, F. Paredes, F. Martín, “High-density microwave encoders for motion control and near-field chipless-RFID”, *IEEE Sensors J*., vol.19, no. 10, pp. 3673-3682, May 2019.
[9] C. Herrojo, J. Mata-Contreras, F. Paredes, Ferran Martín, “Near-Field Chipless RFID Encoders with Sequential Bit Reading and High Data Capacity”, *IEEE MTT-S Int. Microw. Symp*. (IMS’17), Honolulu, Hawaii, Jun. 2017.
[10] C. Herrojo, J. Mata-Contreras, F. Paredes, F. Martín, “High data density and capacity in chipless radiofrequency identification (chipless-RFID) tags based on double-chains of S-shaped split ring resonators (S-SRRs)”, *EPJ Appl. Metamat*., vol. 4, article 8, 6 pages, Oct. 2017.
[11] C. Herrojo, J. Mata-Contreras, F. Paredes, Ferran Martín, “Near-field chipless RFID system with high data capacity for security and authentication applications”, *IEEE Trans. Microw. Theory Techn*., vol. 65 (12), pp. 5298-5308, Dec. 2017.
[12] C. Herrojo, J. Mata-Contreras, F. Paredes, A. Núñez, E. Ramon, and F. Martín, “Near-field chipless-RFID system with erasable/programable 40-bit tags inkjet printed on paper substrates”, *IEEE Microw. Wireless Compon. Lett.*, vol. 28, pp. 272-274, Mar. 2018.
[13] C. Herrojo, J. Mata-Contreras, F. Paredes, A. Núñez, E. Ramón, F. Martín, “Near-field chipless-RFID tags with sequential bit reading implemented in plastic substrates”, *Int. J. Magnetism Magnet. Mat*., vol. 459 pp. 322–327, 2018.
[14] C. Herrojo, M. Moras, F. Paredes, A. Núñez, E. Ramón, J. Mata-Contreras, F. Martín, “Very low-cost 80-bit chipless-RFID tags inkjet printed on ordinary paper”, *Technologies*, vol. 6, p. 52, 2018.
[15] J. Havlicek, C. Herrojo, J. Mata-Contreras, F. Paredes, F. Martín, “Stub-loaded microstrip line loaded with half-wavelength resonators and application to near-field chipless-RFID”, *2018 IEEE MTT-S Latin America Microw. Conf.* (LAMC 2018), Arequipa, Perú, Dec. 12-14, 2018.
[16] J. Havlíček, C. Herrojo, F. Paredes, J. Mata-Contreras, F. Martín, ”Enhancing the per-unit-length data density in near-field chipless-RFID systems with sequential bit reading”, *IEEE Ant. Wireless Propag. Lett*., vol. 18, pp. 89-92, Jan. 2019.
[17] C. Herrojo, F. Paredes, J. Mata-Contreras, E. Ramon, A. Núñez, F. Martín, “Time-domain signature barcodes: near-field chipless-RFID systems with high data capacity” *IEEE Microw. Mag*., to be published.
[18] A. Chamarti and K. Varahramyan, "Transmission delay line based ID generation circuit for RFID applications," *IEEE Microw. Wireless Compon. Lett*., vol. 16, pp. 588-590, 2006.
[19] J. Vemagiri, A. Chamarti, M. Agarwal, and K. Varahramyan, “Transmission line delay-based radio frequency identification (RFID) tag,” *Microw. Opt. Technol. Lett*., vol. 49, no. 8, pp. 1900–1904, Aug. 2007.
[20] M. Schüßler, C. Damm, and R. Jakoby, “Periodically LC loaded lines for RFID backscatter applications,” *Proc. Metamaterials 2007*, Rome, Italy, October 2007, pp. 103-106.
[21] M. Schüßler, C. Damm, M. Maasch, and R. Jakoby, “Performance evaluation of left-handed delay lines for RFID backscatter applications,” *IEEE MTT-S Int. Microw. Symp. 2008*, pp. 177-180.
[22] F.J. Herraiz-Martínez, F. Paredes, G. Zamora, F. Martín, and J. Bonache, “Printed magnetoinductive-wave (MIW) delay lines for chipless RFID applications”, *IEEE Trans. Ant. Propag.*, vol. 60, pp. 5075-5082, Nov. 2012.
[23] L. Zhang, S. Rodriguez, H. Tenhunen, and L.-R. Zheng, “An innovative fully printable RFID technology based on high speed time-domain reflections,” *Conference on High Density Microsystem Design and Packaging and Component Failure Analysis, 2006. HDP’06*., Shanghai, China, Jun. 2006, pp. 166–170.
[24] L. Zheng, S. Rodriguez, L. Zhang, B. Shao, and L.-R. Zheng, “Design and implementation of a fully reconfigurable chipless RFID tag using Inkjet printing technology,” *2008 IEEE Int. Symp. Circuits Syst.*, Seattle, USA, May 2008, pp. 1524–1527.
[25] C. Mandel, M. Schussler, M. Maasch, and R. Jakoby, “A novel passive phase modulator based on LH delay lines for chipless microwave RFID applications,” *2009 IEEE MTT-S Int. Microw. Work. Wireless Sensing, Local Positioning, RFID*, Cavtat, Croatia, Sep. 2009, pp. 1–4.
[26] R. Nair, E. Perret, and S. Tedjini, “Temporal multi-frequency encoding technique for chipless RFID applications,” *IEEE MTT-S Int. Microw. Symp.*, Montreal, Canada, Jun. 2012, pp. 1–3.
[27] S. Gupta, B. Nikfal, and C. Caloz, “RFID system based on pulse-position modulation using group delay engineered microwave C-sections,” *2010 Asia-Pacific Microw. Conf.*, Dec. 2010, pp. 203–206.
[28] E. G. Cristal, “Analysis and exact synthesis of cascaded commensurate transmission-line C-Section all-pass networks,” *IEEE Trans. Microw. Theory Tech*., vol. 14, no. 6, pp. 285–291, Jun. 1966.
[29] S. Gupta, B. Nikfal, and C. Caloz, “Chipless RFID system based on group delay engineered dispersive delay structures,” *IEEE Ant. Wirel. Propag. Lett*., vol. 10, no. 2, pp. 1366–1368, Dec. 2011.
[30] R. S. Nair, E. Perret, and S. Tedjini, “Group delay modulation for pulse position coding based on periodically coupled C-sections,” *Annals of Telecommunications*, Aug. 2013, vol. 68, no. 7–8, pp. 447–457.
[31] R. Nair, E. Perret, and S. Tedjini, “Chipless RFID based on group delay encoding,” *2011 IEEE International Conference on RFID-Technologies and Applications*, Sep. 2011, vol. 1, pp. 214–218.
[32] S. Preradovic and N. C. Karmakar, "Chipless RFID: bar code of the future," *IEEE Microw. Mag.*, vol. 11, pp. 87-97, 2010.
[33] S. Preradovic and N. C. Karmakar, *Multiresonator-Based Chipless RFID: Barcode of the Future*, Springer, 2011.
[34] I. Jalaly and I. D. Robertson, “RF barcodes using multiple frequency bands,” *IEEE MTT-S Int. Microw. Symp.*, Long Beach, USA, Jun. 2005, pp. 139–142.
[35] S. Preradovic, I. Balbin, N. C. Karmakar, and G. Swiegers, “A novel chipless RFID system based on planar multiresonators for barcode replacement,” 2008 *IEEE Int. Conf. RFID*, Apr. 2008, pp. 289–296.
[36] S. Preradovic, I. Balbin, N. C. Karmakar, and G. F. Swiegers, "Multiresonator-based chipless RFID system for low-cost item tracking," *IEEE Trans. Microw. Theory Techn.*, vol. 57, pp. 1411-1419, 2009.
[37] S. Preradovic and N. C. Karmakar, "Design of chipless RFID tag for operation on flexible laminates," *IEEE Anten. Wireless Propag. Lett.*, vol. 9, pp. 207-210, 2010.
[38] J. McVay, A. Hoorfar, and N. Engheta, “Space-filling curve RFID tags,” *2006 IEEE Radio Wireless Symp.*, pp. 199–202.
[39] I. Jalaly and D. Robertson, “Capacitively-tuned split microstrip resonators for RFID barcodes,” *2005 European Microwave Conference*, Oct. 2005, vol. 2, pp. 4–7.
[40] H.-S. Jang, W.-G. Lim, K.-S. Oh, S.-M. Moon, and J.-W. Yu, “Design of low-cost chipless system using printable chipless tag with electromagnetic code”, *IEEE Microw. Wireless Compon. Lett.*, vol. 20, pp. 640-642, 2010.
[41] A. Vena, E. Perret, and S. Tedjini, “A fully printable chipless RFID tag with detuning correction technique”, *IEEE Microw. Wireless Compon. Lett.*, vol. 22(4), pp. 209-211, 2012.
[42] A. Vena, E. Perret, and S. Tedjini, “Design of compact and auto-compensated single-layer chipless RFID tag”, *IEEE Trans. Microw. Theory Techn*., vol. 60(9), pp. 2913-2924, Sep. 2012.
[43] A. Vena, E. Perret, and S. Tedjini, “High-capacity chipless RFID tag insensitive to the polarization”, *IEEE Trans. Ant. Propag.*, vol. 60(10), pp. 4509-4515, Oct. 2012.
[44] D. Girbau, J. Lorenzo, A. Lazaro, C. Ferrater, and R. Villarino, “Frequency-coded chipless RFID tag based on dual-band resonators,” *IEEE Ant. Wireless Propag. Lett*., vol. 11, pp. 126–128, 2012.
[45] M. M. Khan, F. A. Tahir, M. F. Farooqui, A. Shamim, H. M. Cheema, "3.56-bits/cm^2 compact inkjet printed and application specific chipless RFID tag," *IEEE Ant. Wireless Propag. Lett*., vol. 15, pp. 1109-1112, 2016.
[46] R. Rezaiesarlak and M. Manteghi, "Complex-natural-resonance-based design of chipless RFID tag for high-density data," *IEEE Trans. Ant. Propag.*, vol. 62, pp. 898-904, Feb. 2014.
[47] M. S. Bhuiyan and N. Karmakar, “A spectrally efficient chipless RFID tag based on split-wheel resonator,” in *Int. Antenna Technol.*

Workshop on Small Antennas, Novel EM Struct., Mater., Appl., 2014, pp. 1–4.
[48] C. M. Nijas *et al*., “Low-cost multiple-bit encoded chipless RFID tag using stepped impedance resonator,” *IEEE Trans. Ant. Propag*., vol. 62, no. 9, pp. 4762–4770, Sep. 2014.
[49] J. Machac and M. Polivka, “Influence of mutual coupling on performance of small scatterers for chipless RFID tags,” *24th Int. Radioelektron. Conf*., 2014, pp. 1–4.
[50] M. Khaliel, A. El-Awamry, A. Fawky, M. El-Hadidy, and T. Kaiser, “A novel co/cross-polarizing chipless RFID tags for high coding capacity and robust detection,” *2015 IEEE Int. Symp. Ant. Propag. & USNC/URSI National Radio Sci. Meeting*, Jul. 2015, pp. 159–160.
[51] M. Svanda, J. Machac, M. Polivka, J. Havlicek., "A comparison of two ways to reducing the mutual coupling of chipless RFID tag scatterers," in Proc. of *21st International Conference on Microwave, Radar and Wireless Communications (MIKON)*, May 2016, pp. 1-4.
[52] C. Herrojo, J. Naqui, F. Paredes and F. Martín, “Spectral signature barcodes based on S-shaped Split ring resonators (S-SRR)”, *EPJ Applied Metamaterials*, vol. 3, pp. 1-6, Jun. 2016.
[53] A. Vena, E. Perret, S. Tedjini, "Chipless RFID tag using hybrid coding technique," *IEEE Trans. Microw. Theory Techn.*, vol. 59, pp. 3356-3364, Dec. 2011.
[54] A. Vena, E. Perret, S. Tedjini, “A compact chipless RFID tag using polarization diversity for encoding and sensing”, *2012 IEEE Int. Conf. RFID*, pp. 191-197, 2012.
[55] M. A. Islam and N. C. Karmakar, "A novel compact printable dual-polarized chipless RFID system," *IEEE Trans. Microw. Theory Techn.*, vol. 60, pp. 2142-2151, Jul. 2012.
[56] I. Balbin, N.C. Karmakar, “Phase-encoded chipless RFID transponder for large scale low cost applications”, *IEEE Microw. Wireless. Compon. Lett*., vol. 19, pp. 509-511, 2009.
[57] S. Genovesi, F. Costa, A. Monorchio, G. Manara, “Chipless RFID tag exploiting multifrequency delta-phase quantization encoding”, *IEEE Ant. Wireless Propag. Lett.*, vol. 15, pp. 738-741, 2015.
[58] O. Rance, R. Siragusa, P. Lemaitre-Auger, and E. Perret, “RCS magnitude coding for chipless RFID based on depolarizing tag,” in *IEEE MTT-S Int. Microw. Symp. Dig*., 2015, pp. 1–4.
[59] O. Rance, R. Siragusa, P. Lemaître-Auger, E. Perret, "Toward RCS magnitude level coding for chipless RFID," *IEEE Trans. Microw. Theory Techn.*, vol. 64, pp. 2315-2325, Jul. 2016.
[60] C. Herrojo, J. Naqui, F. Paredes, F. Martín, “Spectral signature barcodes implemented by multi-state multi-resonator circuits for chipless RFID tags”, *IEEE MTT-S International Microwave Symposium* (IMS’16), San Francisco, May 2016.
[61] C. Herrojo, F. Paredes, J. Mata-Contreras, S. Zuffanelli and F. Martín, “Multi-state multi-resonator spectral signature barcodes implemented by means of S-shaped split ring resonators (S-SRR)”, *IEEE Trans. Microw. Theory Techn.*, vol. 65, no. 7, pp. 2341-2352, Jul. 2017.
[62] C. Feng, W. Zhang, L. Li, L. Han, X. Chen, and R. Ma, “Angle-based chipless RFID tag with high capacity and insensitivity to polarization,” *IEEE Trans. Ant. Propag*., vol. 63, no. 4, pp. 1789–1797, Apr. 2015.
[63] A. El-Awamry, M. Khaliel, A. Fawky, M. El-Hadidy, and T. Kaiser, “Novel notch modulation algorithm for enhancing the chipless RFID tags coding capacity,” in *IEEE Int. RFID Conf*., 2015, pp. 25–31.
[64] A. Vena, A. A. Babar, L. Sydanheimo, M. M. Tentzeris, and L. Ukkonen, “A novel near-transparent ASK-reconfigurable inkjet-printed chipless RFID tag,” *IEEE Ant. Wireless Propag. Lett*., vol. 12, pp. 753–756, 2013.
[65] D.M. Pozar, *Microwave Engineering*, 4th Ed., John Wiley, Hoboken, NJ, 2011.


Cristian Herrojo was born in Barcelona, Spain, in 1983. He received the Telecommunications Technical Engineering degree in electronic systems and Telecommunications Engineering degree from the Universitat Autònoma de Barcelona in 2010 and 2012, respectively and the PhD degree in Electronics Engineering from the same university in 2018. His research interests include RF/microwave devices, Chipless-RFID and RFID technology, and Metamaterials.


Ferran Paredes was born in Badalona (Barcelona), Spain in 1983. He received the Telecommunications Engineering Diploma (specializing in Electronics) and the Telecommunications Engineering degree from the Universitat Autònoma de Barcelona in 2004 and 2006, respectively and the PhD degree in Electronics Engineering from the same university in 2012. He was Assistant Professor from 2006 to 2008 at the Universitat Autònoma de Barcelona, where he is currently working as a Research Assistant. His research interests include metamaterial concepts, passive microwaves devices, antennas and RFID.


Ferran Martín (M’04-SM’08-F’12) was born in Barakaldo, Spain, in 1965. He received the B.S. degree in physics and Ph.D. degree from the Universitat Autònoma de Barcelona (UAB), Barcelona, Spain, in 1988 and 1992, respectively. From 1994 to 2006 he was Associate Professor in Electronics at the Departament d’Enginyeria Electrònica (Universitat Autònoma de Barcelona), and since 2007 he is Full Professor of Electronics. His research activity has been very broad, including the modelling and simulation of electron devices for high frequency applications, millimeter wave and THz generation systems, the application of electromagnetic bandgaps to microwave and millimeter wave circuits, and the application of metamaterial concepts to the miniaturization and optimization of microwave circuits and antennas. He is now very active in the development of microwave sensors for dielectric characterization and motion control, and also in the topic of chipless-RFID. He is the head of the Microwave Engineering, Metamaterials and Antennas Group (GEMMA Group) at UAB, and director of CIMITEC, a research Center on Metamaterials supported by TECNIO (Generalitat de Catalunya). He has organized several international events related to metamaterials, including Workshops at the IEEE International Microwave Symposium (years 2005 and 2007) and European Microwave Conference (years 2009, 2015, 2017, and 2018), and the Fifth International Congress on Advanced Electromagnetic Materials in Microwaves and Optics (Metamaterials 2011), where he has acted as chair of the Local Organizing Committee. He has acted as Guest Editor in several Special Issues, mainly related to Metamaterials, in various International Journals. He has authored and co-authored over 580 technical conference, letter, journal papers and book chapters, he is co-author of the book on Metamaterials entitled *Metamaterials with Negative Parameters: Theory, Design and Microwave Applications* (John Wiley & Sons Inc. 2008), author of the book *Artificial Transmission Lines for RF and Microwave Applications* (John Wiley & Sons Inc. 2015), co-editor of the book *Balanced Microwave filters* (John Wiley & Sons Inc. and IEEE-Press, 2018), and co-author of the book *Time-Domain Signature Barcodes for Chipless-RFID and Sensing Applications* (Springer, to be published in 2020). Ferran Martín has generated 19 PhDs, he has filed several patents on metamaterials, and he has headed dozens of Development Contracts.
Prof. Martín is a member of the IEEE Microwave Theory and Techniques Society (IEEE MTT-S). He is reviewer of the *IEEE Transactions on Microwave Theory and Techniques* and *IEEE Microwave and Wireless Components Letters*, among many other journals, and he serves as member of the Editorial Board of *IET Microwaves, Antennas and Propagation*, *International Journal of RF and Microwave Computer-Aided Engineering* and *Sensors*. He is also a member of the Technical Committees of the European Microwave Conference (EuMC) and International Congress on Advanced Electromagnetic Materials in Microwaves and Optics (Metamaterials). Among his distinctions, Ferran Martín has received the 2006 Duran Farell Prize for Technological Research, he holds the *Parc de Recerca UAB – Santander* Technology Transfer Chair, and he has been the recipient of three ICREA ACADEMIA Awards (calls 2008, 2013 and 2018). He is Fellow of the IEEE since 2012 and Fellow of the IET since 2016.